CORA Cork Open Research Archive
Cartlann Taighde Oscailte Chorcaí

Title	Electronic and excitonic properties of ultrathin (In,Ga)N layers: the role of alloy and monolayer width fluctuations
Authors	Tanner, Daniel S. P.;Schulz, Stefan
Publication date	2020-09-30
Original Citation	Tanner, D. S. P. and Schulz, S. (2020) 'Electronic and excitonic properties of ultrathin (In,Ga)N layers: the role of alloy and monolayer width fluctuations', Nanoscale, 12, pp. 20258-20269. doi: 10.1039/d0nr03748f
Type of publication	Article (peer-reviewed)
Link to publisher's version	10.1039/d0nr03748f
Rights	© 2020, the Authors. Publication rights licensed to the Royal Society of Chemistry. All rights reserved.
Download date	2026-11-06 06:36:17
Item downloaded from	https://hdl.handle.net/10468/10936



UCC
University College Cork, Ireland
Coláiste na hOllscoile Corcaigh

Electronic and excitonic properties of ultrathin (In,Ga)N layers: The role of alloy and monolayer width fluctuations

Daniel Tanner[1] and Stefan Schulz[2]

[1] *Laboratoire SPMS , CNRS-Centrale Supelec, Universite Paris-Saclay, 91190 Gif-sur-Yvette, France*
[2] *Tyndall National Institute, Lee Maltings, Dyke Parade, Cork T12 R5CP, Ireland*

We present an atomistic theoretical analysis of the electronic and excitonic properties of ultrathin, monolayer thick wurtzite (In,Ga)N embedded in GaN. Our microscopic investigation reveals that (i) alloy fluctuations within the monolayer lead to carrier localization effects that dominate the electronic and optical properties of these ultrathin systems and that (ii) excitonic binding energies in these structures exceed the thermal energy at room temperature, enabling excitonic effects persist even at elevated temperatures. Our theoretical findings are consistent with, and provide an explanation for, literature experimental observations of (i) broad photoluminescence linewidth and (ii) excitonic effects contributing to the radiative recombination process at elevated temperatures. When accounting for small structural inhomogeneities, such as local thickness fluctuations of one monolayer, "indirect" excitons may be found, with electrons and holes independently localized in different spatial positions. This result also provides further arguments for the experimentally observed effects such as (i) non-exponential decay curves in time dependent photoluminescence spectra and (ii) the "S"-shape temperature dependence of the photoluminescence peak energies. Overall, our results provide fundamental understanding, on an atomistic level, of the electronic and optical properties of ultrathin, quasi 2D (In,Ga)N monolayers embedded in GaN, and offer guidance for the tailoring of their properties for potential future device applications.

I. INTRODUCTION

Over recent years there has been a strong drive in understanding and designing novel materials with new and exciting properties, for both the furtherance of our insight into fundamental physics and also from an applications point of view.[1–4] For instance, 2D materials have generated great scientific interest due to their potential for flexible band gap engineering and higher carrier mobilities compared to more conventional systems.[5,6] Over the last few years more and more materials have been theoretically predicted and found experimentally.[1,3]

Recently, research focus has also shifted towards realizing monolayer (ML) structures based on more conventional semiconductor materials such as InN, GaN or AlN.[7–11] These III-N materials are key building blocks for modern light emitting devices.[12] In the visible spectral region, (In,Ga)N quantum well (QW) systems have attracted considerable interest for applications in such diverse areas as light emitting diodes,[13] solar cells[14] or photoelectrochemical water splitting devices[15].

By realizing 2D versions of (In,Ga)N or III-N materials in general, their electronic and optical properties can significantly be modified.[8] In the case of InN for instance, 2D/ML systems have been targeted experimentally by embedding them in a host matrix of GaN.[7,9,16–18] The benefits of such an approach are manifold. Firstly, having ML thick InN layers embedded in GaN, the spatial separation of electron and hole wave functions, due to built-in polarization fields,[19] are ideally eliminated. This is of central importance to enhance the radiative recombination rate in comparison to "conventional" *c*-plane (In,Ga)N/GaN systems, and thus efficient light emission.[20] Secondly, given that carrier localization effects are very pronounced in (In,Ga)N-based structures,[21–24] and this feature is widely assumed to be the reason why these systems emit light efficiently despite their high defect densities,[25] even ML (In,Ga)N structures could still prevent carriers from reaching defects in the material and thus suppress non-radiative recombination. Additionally, the carrier confinement in 2D (In,Ga)N systems is strongly increased compared to "conventional" *c*-plane QWs. This is expected to lead to increased excitonic binding energies, which ideally prevent thermal dissociation at room temperature. Finally, the increased exciton binding energies and the reduction of the spatial separation of carriers may also reduce the electron phonon coupling, which in turn may allow to reduce phonon assisted Auger recombination effects.[26]

However, it has already been highlighted that there are fundamental limitations to growing such a 2D system.[27] These studies show that a maximum of 25% In can be incorporated in an ML that ideally should be 100% In coherently grown on GaN.[27] Also, while recent experimental investigations[9,28] on these"quasi 2D" (In,Ga)N layers reveal effects which are consistent with the ideally expected properties of a 2D (In,Ga)N system (e.g. excitonic recombination at elevated temperatures), there are also findings that are more consistent with "standard" *c*-plane (In,Ga)N/GaN QW systems (e.g. non-exponential decay transients in time resolved PL spectra). While experiments have started to shed light onto the properties of these ultrathin heterostructures, far less attention has been directed towards the theoretical description of the electronic and optical properties of these novel systems. The theoretical description is very challenging given that one is (i) not dealing with pure InN or GaN and that (ii) the (In,Ga)N MLs are embedded in GaN and not in vacuum. Thus large supercells are required to account the GaN barrier and alloy fluctuations within an (In,Ga)N

ML. Additionally, due to the strong carrier confinement, excitonic effects have to be considered. Therefore, standard first-principle studies, which capture all the above discussed factors to achieve a detailed description of the electronic and optical properties are basically impossible, given the large supercell size required.

In this work, we address the electron and excitonic properties of ultrathin (In,Ga)N layers embedded in GaN in the combined framework of atomistic tight-binding theory and configuration interaction calculations. The results from our atomistic many-body analysis show that (i) carrier localization effects are very important to describe the electronic and optical properties of these ultrathin systems and that (ii) excitonic effects are very pronounced in this quasi 2D material. Our theoretical findings are in line with and provide further insight into the experimental observations of broad PL spectra and pronounced excitonic effects contributing to the radiative recombination process at elevated temperatures in ML thick (In,Ga)N systems. Our calculations also demonstrate that small structural inhomogeneities can significantly affect their optical properties and may lead to the appearance of "indirect" excitons,[29,30] meaning that the Coulomb correlated electrons and holes are localized in different spatial regions of the ML system. This situation of "independently" localized carriers[31] is consistent with the experimental observation of non-exponential decay transients in quasi 2D (In,Ga)N MLs.[9,28] Also, our theoretical findings, given the strong variation in the ground state transition energies and the appearance of indirect excitons are in line with the experimental observation of an "S"-shape temperature dependence of the PL peak energies.[9,28] Overall, our results provide on an atomistic level fundamental understanding of the electronic and optical properties of ultrathin, quasi 2D (In,Ga)N MLs embedded in GaN, and thus provide guidance to tailor their properties for potential future device applications.

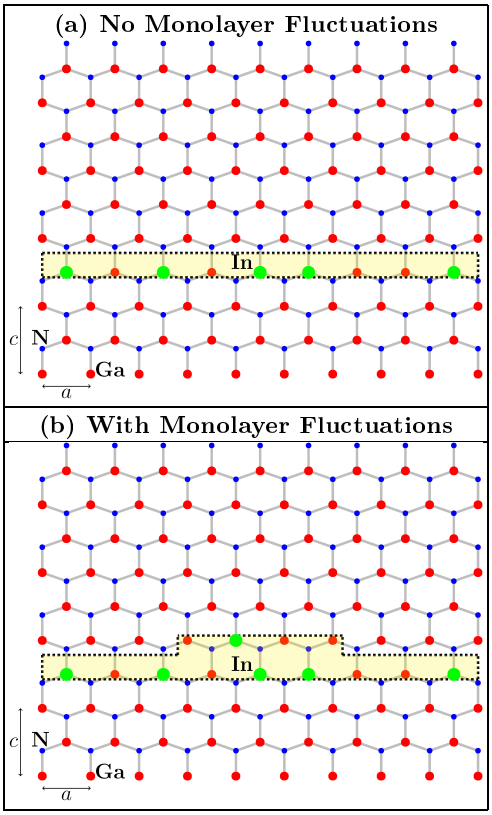


FIG. 1. Schematic illustration of ultrathin (In,Ga)N layers studied in this work. (a) Quasi-2D atomically "flat" (In,Ga)N monolayer embedded in GaN. (b) Same as in (a) but with In atom penetration into the GaN barrier in a small spatial region of the supercell. Here, penetration into only one additional monolayer is allowed.

II. RESULTS

In this section we present the results of our theoretical study. All calculations have been performed on supercells with a size of approximately $20 \times 18 \times 10\,\mathrm{nm}^3$ ($\approx 328,000$ atoms), allowing therefore to study in-plane carrier localization due to alloy fluctuations in an $In_{0.25}Ga_{0.75}N$ ML. To rigorously analyze the impact of the alloy microstructure on the results, 20 different microscopic configurations have been generated. Bearing in mind the fundamental limit of In content in a single ML embedded in GaN,[27] we focus our attention on systems with 25% In. Furthermore, for all structures a random alloy assumption has been made. More information about this assumption and the supercells used in our study are given in the Section "Methods: Model geometry" further below.

Before studying $In_{0.25}Ga_{0.75}N$ ML systems, we first discuss $In_{0.25}Ga_{0.75}N$ *bulk* systems. This provides general insight into the combined impact of alloy fluctuations and Coulomb effects on the electronic and optical properties of (In,Ga)N systems. In a second step we analyze the electronic properties of an atomically "flat" ML of $In_{0.25}Ga_{0.75}N$ embedded in GaN. Thirdly, we study the impact of structural inhomogeneities, where we consider In atoms "bleeding" into a small spatial region of the GaN barrier material. Such a penetration of In atoms is only allowed for a second ML of $In_{0.25}Ga_{0.75}N$ and in a disk-like area with a radius of approximately 2.5 nm. A schematic illustration of the situations studied is given Fig. 1, where Fig. 1 (a) shows the atomically "flat" layer and (b) the system in which the In atoms are allowed to penetrate into the GaN barrier. For the sake of simplifying, for instance, the visualization of charge densities, the ML fluctuations are always placed near the (in-plane) center of the simulation cell. More detailed discussions on these small thickness fluctuations are given below in the Section "Methods: Model geometry".

The electronic and excitonic properties of the systems have been calculated in the combined framework of atomistic tight-binding (TB) theory and configuration interaction (CI) calculations. This allows us to study excitonic

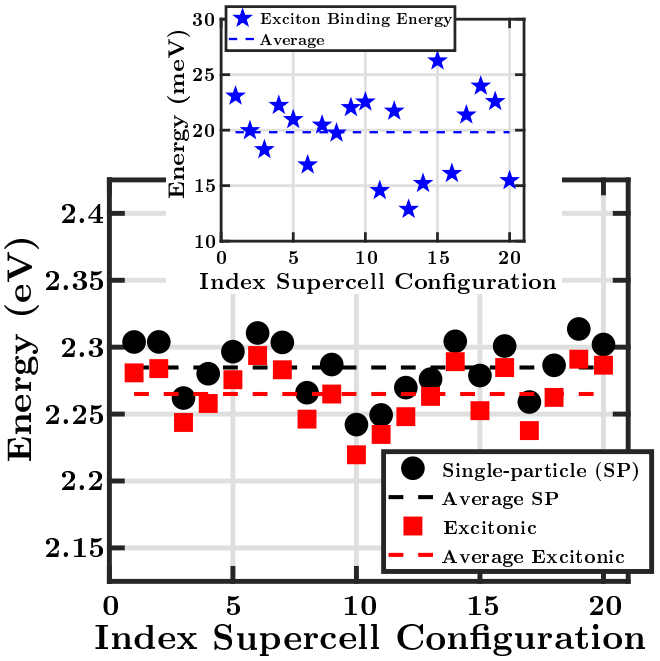


FIG. 2. Emission energies for bulk wurtzite $In_{0.25}Ga_{0.75}N$. The data are displayed as a function of the index of the supercell configurations (microscopic alloy configurations). The single-particle transition energies are given by the black circles; the excitonic ground state emission energies are denoted by the red circles. The average energies are given by the dashed horizontal lines. Inset: Exciton binding energy E_X^b for bulk wurtzite $In_{0.25}Ga_{0.75}N$. The data are again displayed as a function of the index of the supercell configurations (microscopic alloy configurations). The average binding energy, $\tilde{E}_X^{b,\mathrm{bulk}}$, is given by the horizontal dashed line.

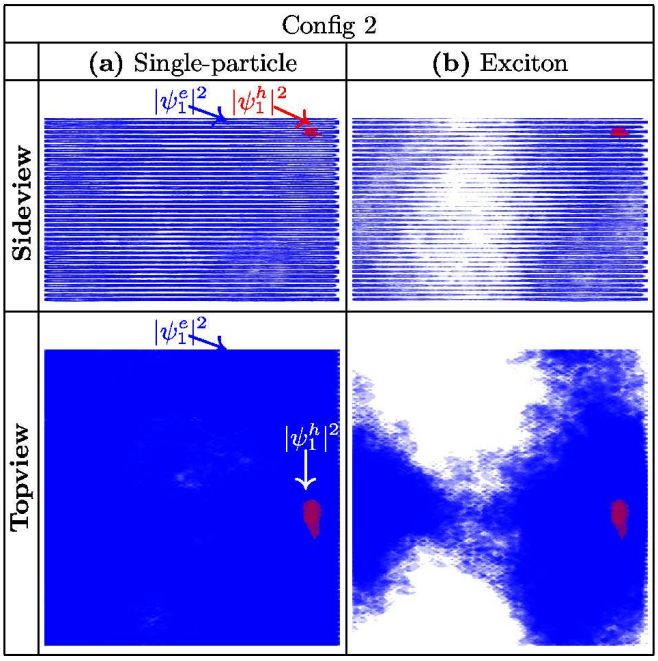


FIG. 3. (a) Isosurface plots of the electron $|\psi^e_{\mathrm{GS}}|^2$ (blue) and hole $|\psi^h_{\mathrm{GS}}|^2$ (red) ground state charge densities in a bulk (In,Ga)N system with 25% In; (b) shows results when excitonic effects are taken into account. The isosurface plots are depicted at 10% of respective maximum charge density values. The data are displayed for and arbitrarily selected microscopic alloy configuration (Config), here Config 2.

properties through an increasingly more complex many-body treatment, where we start from the single-particle approach and finally culminate in the CI method that goes beyond ground state properties of the disordered energy landscape in terms of a single-particle description. More details on the theoretical framework are given in the Section "Methods: Theoretical Framework".

A. Electronic and optical properties of (In,Ga)N bulk systems

Starting with bulk systems, we first analyze the impact of the alloy microstructure on the emission wavelength and the exciton binding energy. Figure 2 displays the single-particle (no Coulomb effects included) and excitonic ground state transition energies as a function of the index of the supercell configurations (microscopic alloy configurations). As this figure reveals, the alloy microstructure significantly affects the transition energies, given that the transition energy varies significantly with configuration number. Including excitonic effects in the calculations, the attractive Coulomb interaction between electron and hole leads to a red-shift of the transition energy. The excitonic binding energy, calculated as the difference between the single-particle and excitonic ground state transition energy, is depicted in the inset of Fig. 2. The data shows that the excitonic binding energy also noticeably depends on the alloy microstructure. On average we find an excitonic binding energy $\tilde{E}_X^{b,\mathrm{bulk}}$ of 20 meV, which is lower than the binding energy reported for pure GaN ($E_X^{b,\mathrm{GaN}}$=23-28 meV),[32] but significantly larger when compared to values reported for pure InN ($E_X^{b,\mathrm{InN}}$=5-6 meV).[33,34]

To shed more light onto the question of why the alloy microstructure affects the transition energies, Fig. 3 (a) depicts isosurface plots of electron $|\psi^e_{\mathrm{GS}}|^2$ (blue) and hole $|\psi^h_{\mathrm{GS}}|^2$ (red) ground state (GS) single-particle (no excitonic effects) charge densities for a sideview perpendicular to the wurtzite c-axis (upper row), and a topview parallel to the c-axis (lower row) for an arbitrarily chosen microscopic alloy configuration (Config), here Config 2. These isosurfaces are visualized at 10% of the respective maximum charge density values. As Fig. 3 clearly reveals, random alloy fluctuations in (In,Ga)N bulk systems are sufficient to strongly localize the hole wave functions. The electron ground state is more delocalized, but also reveals perturbations to the otherwise expected delocalized Bloch wave function nature. Overall, the arbitrarily chosen alloy configuration reflects the behavior also found in

the remaining 19 microscopic configurations. The result of a strong hole and less pronounced electron localization effect due to alloy fluctuations is consistent with density functional theory (DFT) and empirical pseudopotential studies on bulk (In,Ga)N systems.[21,23]

When including excitonic effects in the calculation, we find that the electron wave function starts to localizes about the hole, which remains localized in the same position, as Fig. 3 (b) shows. Similar situations are observed in the other alloy configurations studied. This result is in agreement with the widely accepted explanation of why III-nitride based materials can be used as efficient light emitters despite their large defect densities:[25] localization effects prevent the carriers from reaching defects where they would recombine non-radiatively.

Having discussed general aspects of carrier localization effects in (In,Ga)N materials, we turn now and study the impact of alloy fluctuations and Coulomb effects on the electronic and optical properties of quasi 2D (In,Ga)N/GaN MLs. In a first step, Sec. II B, we analyze the electronic and excitonic properties of atomically "flat" ML systems, cf. Fig. 1 (a). In Sec. II C, we focus our attention on the system with small structural inhomogeneities, cf. Fig. 1 (b).

B. Electronic and optical properties of monolayer thick (In,Ga)N

The single-particle ground state transition energy (black circles) of an $In_{0.25}Ga_{0.75}N$ ML embedded in GaN is displayed in Fig. 4 as a function of the index of the supercell configurations (microscopic alloy configurations); the black dashed line gives the average transition energy. Similarly to the bulk system discussed above, we find that for the ML system the ground state transition energy varies strongly with microscopic alloy configuration. Thus even for the ML thick $In_{0.25}Ga_{0.75}N$/GaN system, the alloy microstructure of the layer strongly affects the electronic and optical properties. We also find that compared to the bulk system, cf. Fig. 2, the single-particle transition energies are shifted to larger energies, due to carrier confinement. We will come back to this aspect further below.

Turning to the excitonic ground state emission energy (red squares), our calculations show that this quantity also depends on the alloy microstructure in the layer as it varies noticeably with configuration number. Overall, this strong dependence of the emission energy on the alloy microstructure is commensurate with a broad PL linewidth.[35] The experimental studies of Ma *et al.*[9] and Anikeeva *et al.*[28] on quasi 2D $In_{0.25}Ga_{0.75}N$ layers reveal such broad PL linewidth. We note that in "conventional/standard" *c*-plane (In,Ga)N/GaN QWs, the broad PL linewidth is usually attributed to strong hole localization effects due to (random) alloy fluctuations, while the electron wave function exhibits a more delocalized character and is less affected by the alloy microstructure.[22,35]

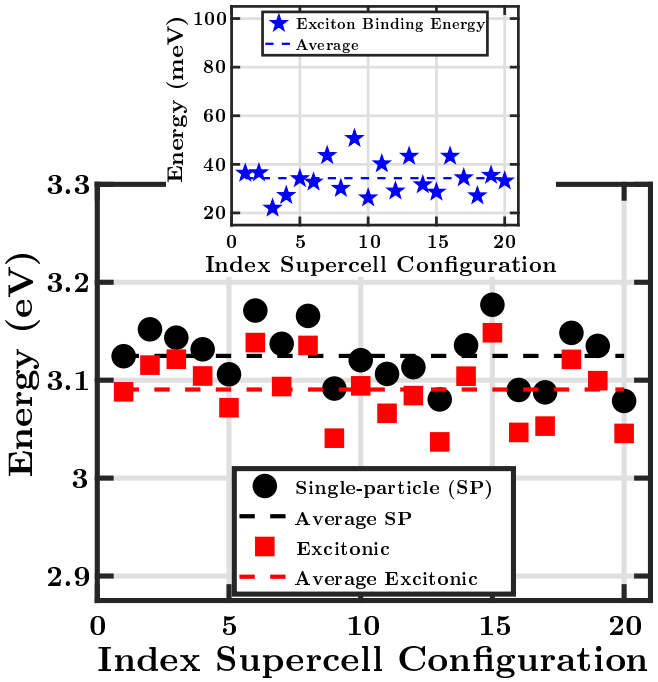


FIG. 4. Emission energies of a monolayer thick wurtzite $In_{0.25}Ga_{0.75}N$ layer embedded in GaN. The data are displayed as a function of the index of the supercell configurations (microscopic alloy configurations). The single-particle transition energies are given by the black circles; the excitonic ground state emission energies are denoted by the red squares. The average energies are given by the dashed horizontal lines. Inset: Exciton binding energy E_X^b as a function of the index of the supercell configurations (microscopic alloy configurations). The average binding energy, $\tilde{E}_X^b$, is given by the horizontal dashed line.

We will further discuss these aspects in the context of ultrathin (In,Ga)N layers below. But before this, we turn to analyze excitonic effects in more detail.

Comparing the single-particle and excitonic transition energies, we find that Coulomb effects give rise to a significant red-shift in the transition energies, thus large excitonic binding energies. Following our approach for the bulk system, the exciton binding E_X^b energy is calculated as the difference between the single-particle and the excitonic ground state transition energies. The resulting binding energies are given in the inset of Fig. 4 as a function of the index of the supercell configurations (microscopic alloy configurations); the dashed line denotes the average excitonic binding energy $\tilde{E}_X^b$; we find a value of $\tilde{E}_X^b \approx 35$ meV. The inset also clearly reveals that the magnitude of E_X^b depends on the microscopic alloy configuration. Values exceeding 50 meV (e.g. Config 9) as well as below 25 meV (e.g. Config 3) are found. Overall, we observe that compared to the bulk system, excitonic effects are significantly increased. We attribute this again to the increased carrier confinement in the ML case. It is also important to note that the calculated average binding energy, $\tilde{E}_X^b \approx 35$ meV, is larger than the

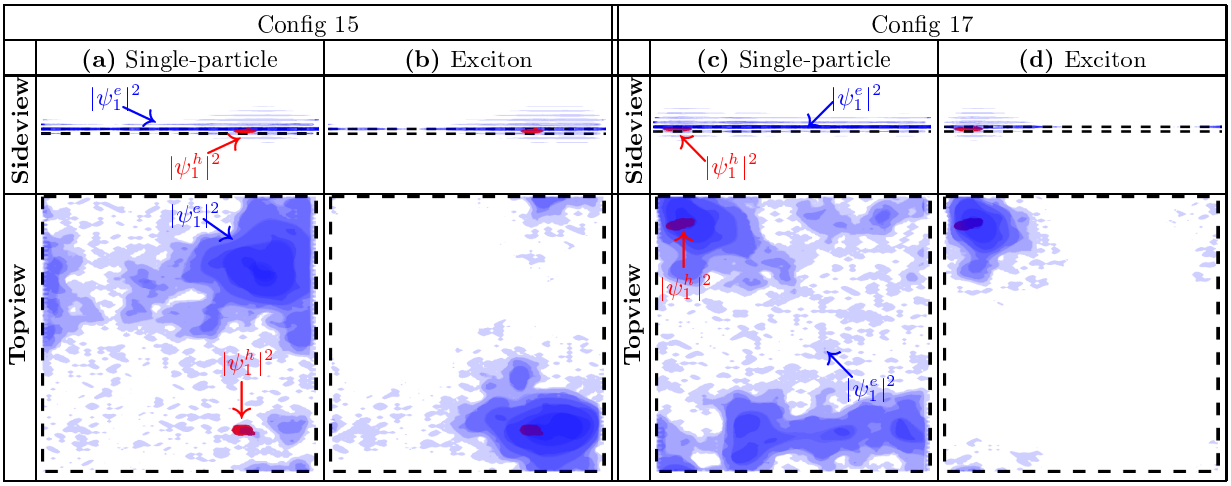


FIG. 5. Isosurface plots of the electron $|\psi^e_{\rm GS}|^2$ (blue) and hole $|\psi^h_{\rm GS}|^2$ (red) ground state charge densities for the alloy configuration (Config) 15 and Config 17. The data are shown for the atomically "flat" (no width fluctuations) (In,Ga)N monolayer system with 25% In. The isosurfaces correspond to 10% of respective maximum charge density values (Note that the different shades in the isosurface plots of the charge densities originate from overlapping isosurfaces stemming from different planes in c-direction). (a) and (c) depict the single-particle results for Config 15 and Config 17, while (b) and (d) display the data for Config 15 and Config 17 when including excitonic effects in the calculations. The dashed lines in the sideview are placed slightly above/below the InGaN ML region to indicate the region where In atoms are present. In the topview the dashed lines indicate supercell boundary.

thermal energy at room temperature; therefore, excitonic recombination at elevated temperature can be expected. This conclusion is supported by the experimental studies on quasi 2-D (In,Ga)N/GaN ML systems.[9]

In order to analyze carrier confinement effects in more detail and to study the interplay of carrier localization effects and Coulomb interaction in quasi 2D $In_{0.25}Ga_{0.75}N$ ML systems further, we look at the electron and hole ground state charge densities. Similarly to Fig. 3, Fig. 5 displays isosurface plots of the single-particle electron $|\psi^e_{\rm GS}|^2$ (blue) and hole $|\psi^h_{\rm GS}|^2$ (red) ground state charge densities for (a) the alloy configuration (Config) 15 and (c) Config 17. The isosurfaces are plotted at 10% of the respective maximum charge density values. The upper panel in Fig. 5 always shows the results for a sideview perpendicular to the wurtzite c-axis, while the lower panel depicts the data for a topview parallel to the c-axis. These two configurations have been selected on the basis that they represent situations below (Config 15) or close (Config 17) to the average exciton binding energy of $\tilde{E}^b_X \approx 35$ meV.

Before turning to the impact of the Coulomb interaction on the results, several features of the single-particle charge densities are already of interest. Firstly, the sideview (upper row in Fig. 5) clearly indicates that the (In,Ga)N ML leads to a strong localization of electrons and holes in and around this layer. These results are consistent with the DFT calculations in Ref.[28], which also indicate strong carrier localization effects as the barrier width between (In,Ga)N MLs increases. Secondly, when looking at the topview (lower row in Fig. 5) we find that the hole is much more strongly localized than the electron wave function. Overall, the behavior of very strongly localized hole states and a more delocalized electron state seen in the chosen alloy configuration reflects the behavior also found in the remaining supercell configurations. This is consistent with theoretical results on conventional polar and also non-polar (In,Ga)N/GaN QWs.[22,36] Moreover, we note that previous calculations have already revealed that a single In-N-In chain in a GaN matrix is sufficient to localize hole wave functions.[21,23,37] So even a ML of $In_{0.25}Ga_{075}N$ leads to the presence of such chains and therefore one expects strong hole localization effects in such a system, consistent with our presented results. To shed further light on the localization effects, Fig. 6 displays the contour-plot of the built-in potential of such a ML thick (In,Ga)N system. As Fig. 6 clearly reveals, while the potential drop "across" the structure is very small, locally strong fluctuations in the built-in potential are observed. These local potential "pockets", in conjunction with the large effective hole mass,[38,39] can then lead to strong hole localization effects. The combination of negligible potential drop, Fig. 6, and ML thickness has the desired effect on the electronic structure that in contrast to a conventional c-plane (In,Ga)N/GaN QW system, the spatial separation *along* the c-axis to due to intrinsic built-in fields has been removed in the ML (In,Ga)N/GaN structure. However, when looking at the topview of the charge densities (lower row in Fig. 5) it also becomes clear why (i) the transition energy and (ii) the exciton binding energy is strongly configuration dependent. While for Config. 15 electron and hole localize in different spatial *in-plane* regions, in Config. 17 electron and hole basically "co-localize" in the same po-

sition. Thus one can expect that Config. 17 exhibits a larger exciton binding energy E_X^b when compared to Config. 15. This exactly is the result we observe in Fig. 4 when comparing the calculated exciton binding energies of the two alloy configurations studied in Fig. 5. We also note that to capture the effect of in-plane carrier separation, large supercells are required to avoid artifacts from periodic boundary conditions; therefore calculations performed on smaller supercells may not properly account for the impact of alloy fluctuations and thus the alloy microstructure on the transition/binding energies.

To deduce the impact of excitonic effects on the optical properties, we turn to Fig. 5 (b) and (d) which reveal localization of the electron about the hole for both Config 15 and 17. Thus in the case of the considered atomically "flat" system, one is left with exciton localization effects; we find that this is characteristic for all considered 20 configurations. Experimentally, such an exciton localization should manifest itself in, for instance, single-exponential decay transients in time-resolved PL measurements. Such a characteristic has been observed and discussed in nonpolar (In,Ga)N/GaN QW systems, where the macroscopic electrostatic built-in field is absent.[40,41] However, the experimental studies reported in Ref.[9,28] on ultrathin (In,Ga)N/GaN layers show non-single-exponential decay transients. In fact the observed non-exponential decay transients are similar to standard c-plane (In,Ga)N/GaN QW systems with strong built-in fields.[31,41] In such a standard c-plane (In,Ga)N/GaN QW system the often used explanation is that electrons and hole are independently localized in different spatial positions in the QW due to the combined effect of electrostatic built-in field along the c-axis and alloy fluctuations. Building on this idea and using a donor-acceptor pair model, Morel *et al.*[31] obtained very good agreement between theoretical predictions and measured time-resolved PL data in c-plane (In,Ga)N/GaN QWs. Our calculations on quasi 2D (In,Ga)N layers indicate however a co-localization of electron and hole due to random alloy fluctuations and the attractive Coulomb interaction between electron and hole. This raises the question about other factors affecting the electronic and optical properties of ML thick (In,Ga)N systems embedded in GaN.

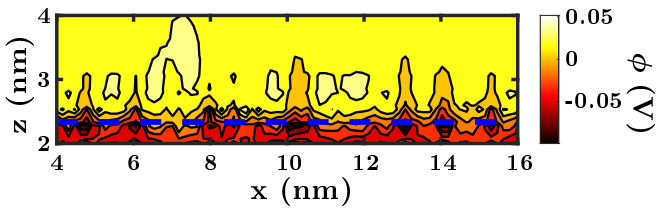


FIG. 6. Contour plot of the built-in potential ϕ in the $x-z$-plane (z-axis parallel to to wurtzite c-axis) for $y = 8.7$ nm. The data is shown for alloy configuration 15 for the atomically "flat" $In_{0.25}Ga_{0.75}N$ monolayer system. The (blue) dashed line indicates the monolayer region in which In atoms are present.

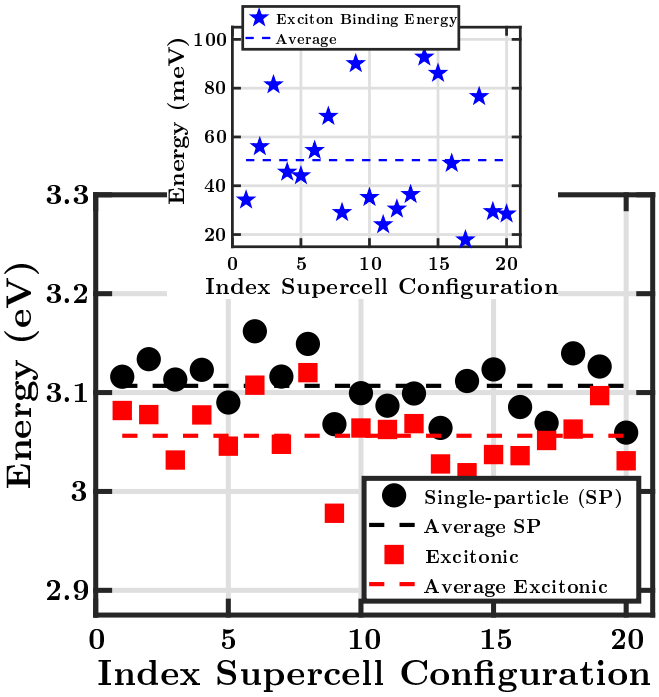


FIG. 7. Emission energies for a monolayer thick wurtzite $In_{0.25}Ga_{0.75}N$ layer embedded in GaN. In the present case In atoms are allowed to "bleed" into the GaN barrier of the (In,Ga)N monolayer system with 25% In. The data are displayed as a function of the index of supercell configurations (microscopic alloy configurations). The single-particle transition energies are given by the black circles; excitonic ground state emission energies are denoted by the red squares. The average energies are given by the dashed horizontal lines. Inset: Exciton binding energy E_X^b as a function of the index of the supercell configurations (microscopic alloy configurations). The average binding energy, $\tilde{E}_X^{b,F}$, is denoted by the horizontal dashed line.

A feature that has been observed in standard c-plane (In,Ga)N/GaN QWs is that In atoms penetrate into the GaN barrier.[42] This penetration may also be spatially dependent so that the well width fluctuates locally.[43,44] These fluctuations in well width have been reported to be of the order of 1-2 MLs in "conventional" c-plane QWs. In the following section we discuss the impact of such inhomogeneities on the electronic and optical properties of $In_{0.25}Ga_{0.75}N$/GaN quasi 2D systems.

C. Electronic and optical properties of monolayer thick (In,Ga)N layers with structural inhomogeneities

In this section we study the electronic and excitonic properties of the $In_{0.25}Ga_{0.75}N$ ML system schematically depicted in Fig. 1 (b), where in a 1 ML thick and disk-shaped (approximately 2.5 nm radius) region above the $In_{0.25}Ga_{0.75}N$ ML In atoms can "bleed" into the GaN barrier. Two aspects of these structural inhomogeneities

are important to note. First, they reflect a very small deviation from the $In_{0.25}Ga_{0.75}N$ ML considered so far, taking into account that the in-plane dimensions of the simulation cell are 20 nm× 18 nm. Secondly, since we assume random alloy fluctuations, the number of In atoms in the barrier and their spatial arrangement vary from configuration to configuration. Thus the resultant width fluctuation is not a perfectly disk-shaped object; we only allow for the presence of In atoms in a disk-like region in the GaN barrier material, with the alloy fluctuations characteristic of this In content producing a variety of shapes. Further discussions are given in the Section "Methods: Model geometry".

Figure 7 shows the single-particle ground state transition energy (black circles) for the system with structural inhomogeneities as a function of the index of the supercell configurations (microscopic alloy configurations). Overall, when comparing the single-particle energy gaps depicted in Fig. 4 (no ML fluctuations) and Fig. 7 (with ML fluctuations), we observe that the transition energies are shifted to smaller energies when ML fluctuations are present. We attribute this behavior to the slight increase in the "volume" of the ML system. However, compared to bulk systems, Fig. 2, the strong carrier confinement along the c-axis still leads to much larger transition energies in the ML system. Overall, and similar to the structure without width fluctuations, Fig. 7 clearly shows a strong dependence of the single-particle transition energy on the configuration number and thus the alloy microstructure. The same behavior is reflected in the excitonic ground state transition energy, given in Fig. 7 by the red squares. Thus, as already discussed above, these fluctuations in the transition energy will manifest in broad PL spectra, consistent with the measurements on quasi 2D (In,Ga)N/GaN MLs.[9,28] Compared to the atomically "flat" structures, we observe that excitonic effects are enhanced when introducing thickness fluctuations. This is reflected in the average excitonic binding energy $\tilde{E}_X^{b,F}$ depicted in the inset of Fig. 7, and when compared to the binding energy $\tilde{E}_X^b$ obtained in the absence of width fluctuations. In the absence of width fluctuations $\tilde{E}_X^b \approx 35$ meV, while when these fluctuations are present an average excitonic binding energy of $\tilde{E}_X^{b,F} \approx 51$ meV is found. Although the average excitonic binding energy in the system with ML width fluctuations is larger, we also find configurations (e.g. Config 17 in Fig. 7) with exciton binding energies below the values observed in the atomically flat $In_{0.25}Ga_{0.75}N$ ML system (cf. Fig. 4).

To further investigate the question of why in general excitonic effects are enhanced in the system with ML width fluctuations, we study electron $|\psi^e_{\rm GS}|^2$ and hole $|\psi^h_{\rm GS}|^2$ single-particle ground state charge densities. Isosurface plots of $|\psi^e_{\rm GS}|^2$ (blue) and $|\psi^h_{\rm GS}|^2$ (red) are depicted in Fig. 8 (a) and (c) for Config. 15 and Config. 17 at 10% of the respective maximum charge density values. These configurations have been selected since they correspond to situations with very large (Config 15; $E_X^{b,F} = 86$ meV) and low (Config 17, $E_X^{b,F} = 18$ meV) exciton binding energies, cf. Fig. 7. The charge densities are shown for a sideview perpendicular (upper row) and a topview along (lower row) the wurtzite c-axis. In a first step we turn our attention to the single-particle electron and hole ground state charge densities of Config 15 (cf. Fig. 8) (a), which exhibits an exciton binding energy of $E_X^{b,F} = 86$ meV. Figure 8 (a) reveals that both electron and hole are localized in the small region of the ML width fluctuation. This behavior is also supported by the built-in potential profile shown in Fig. 9, which reveals especially in the region of ML width fluctuation strong potential fluctuations. These fluctuations present especially for the holes carrier "localization centers". While in Fig. 9 we find a strong potential fluctuation in the region where In atoms "bleed" into the GaN barrier, also away from this region strong fluctuations in the built-in potential are observed. Thus the local alloy environment plays an important role. However, for Config 15 the built-in potential supports a "co-localization" of the carriers, so that the wave function overlap between electron and hole is very large and confined to a small spatial region. Therefore, Coulomb effects are enhanced, as for instance discussed in Ref.[45] for small InN/GaN quantum dots, and a large exciton binding is expected, consistent with our result shown in Fig. 7. Turning now to the single-particle ground state charge densities of Config 17, displayed in Fig. 8 (c), we find a different situation. While the electron wave function is still localized by the ML width fluctuation, the hole wave function is localized in a spatially different region. Since the electron exhibits a lower effective mass in comparison to the hole,[38,39] it is less sensitive to the local alloy fluctuations and connected built-in field fluctuations (cf. Figs. 6 and 9) as the hole, consistent with our discussions on the bulk systems, see Sec. II A. Given that in the single-particle picture electron and hole are localized in very different spatial positions, the wave function overlap is reduced. Therefore, in comparison to Config 15, Coulomb effects are reduced and consequently a reduced exciton binding energy is expected in Config. 17. This effect is also borne out in the exciton binding energies shown in Fig. 7.

In a second step we turn now to the question of how the attractive Coulomb interaction affects electron and hole wave functions. In the absence of ML width fluctuations, cf. Fig. 5, the electron localizes about the hole, so that we are left with the picture of exciton localization. Turning to the system with width fluctuations, our calculations reveal that in this case, the electron is localized in the region where In atoms penetrate the GaN barrier. Looking at Config 15 (Fig. 8 (b)), since electron and hole are already localized in the same spatial position in the absence of excitonic effects (single-particle results, Fig. 8 (a)), this co-localization is slightly increased by the attractive Coulomb interaction. Therefore, for this microscopic configuration one is again left with exciton localization effects.

However, it is also interesting to note that the feature

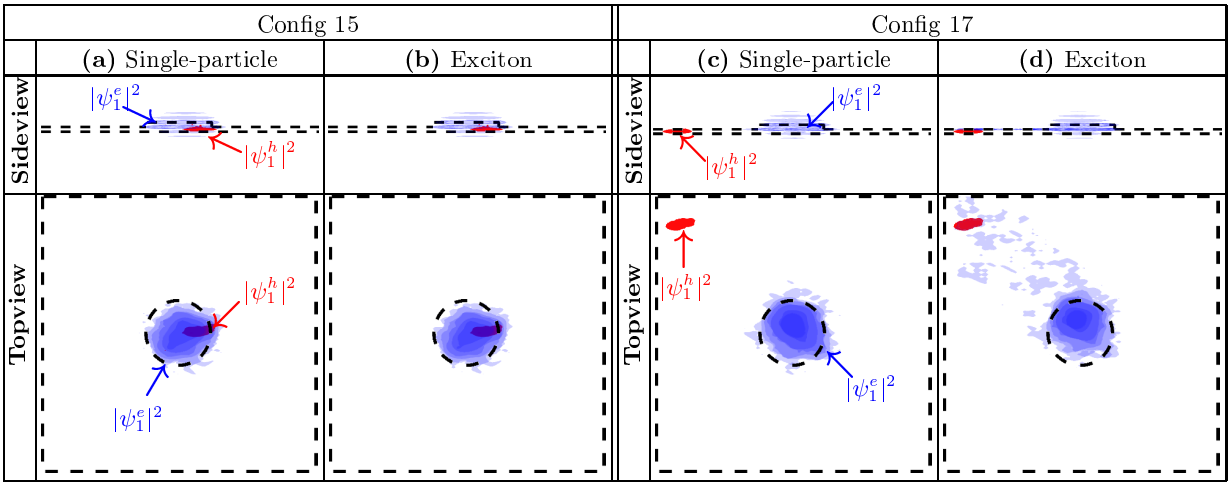


FIG. 8. Isosurface plots of the electron $|\psi^e_{\rm GS}|^2$ (blue) and hole $|\psi^h_{\rm GS}|^2$ (red) ground state charge densities for the microscopic alloy configuration (Config) 15 and Config 17, respectively. In the present case In atoms are allowed to "bleed" into the GaN barrier of the (In,Ga)N monolayer system with 25% In. The isosurfaces are shown at 10% of respective maximum charge density values (Note that the different shades in the isosurface plots of the charge densities originate from overlapping isosurfaces stemming from different planes in c-direction). (a) and (c) depict the single-particle results for Config 15 and Config 17, while (b) and (d) show the data when including excitonic effects in the calculations. The dashed lines indicate the supercell boundary but also the area in which In atoms are allowed to penetrate into the barrier region. The dashed lines in the sideview are place slightly above/below the InGaN ML region to indicate the region in which In atoms are present.

of exciton localization can also arise in a very different form as Fig. 10 reveals for Config 14. While in the single-particle picture, Fig. 10 (a) the electron wave function is mainly localized in the region of the ML width fluctuation, the hole is localized in different spatial position. But, when including Coulomb effects the hole wave function localizes about the electron wave function. We attribute this to the fact that the energy landscape seen by the hole has several different local energy minima, so that it is important to include this aspect in the many-body description, as done by our CI calculation. We note that the behavior of the hole localizing about the electron in the case of our quasi-2-D (In,Ga)N/GaN system is different from for instance observations in non-polar m-plane (In,Ga)N/GaN QW systems previously reported in the literature.[36] These differences may arise due to differences in the underlying strain field (c-plane vs. m-plane) as well as the situation that a wider well in the conventional (In,Ga)N/GaN QW system may lead to a very different potential energy landscape.

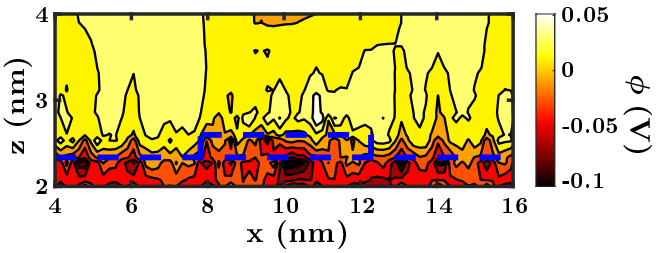


FIG. 9. Contour plot of the built-in potential ϕ in the $x-z$-plane (z-axis parallel to wurtzite c-axis) for $y = 8.7$ nm. In the present case In atoms are allowed to "bleed" into the GaN barrier of the (In,Ga)N monolayer system with 25% In. The (blue) dashed line indicates the monolayer region in which In atoms are present.

We also note that not always do Coulomb effects dominate over carrier localization effects introduced by alloy fluctuations. This becomes clear when turning to Config 17, cf. Fig. 8 (c) and (d), where the situation is different compared to Config 14 and 15. For Config 17, electron and hole are spatially separated in the single-particle picture (cf. Fig. 8 (c)). When including Coulomb effects in the calculations, we find that the attraction is not strong enough to reduce the spatial separation of electron and hole (cf. Fig. 8 (c) and (d)) originating from random alloy introduced carrier localization effects. Therefore, for Config. 17 we are left with an *indirect* exciton[29,30] or *independently* localized carriers.[31,41] When looking at the other configurations (not shown) we find a mixture of these situations (exciton localization and "indirect" excitons); approximately 50% of the studied systems can be classified as "indirect" excitons. Therefore, based on our theoretical results and similar to standard c-plane systems, the radiative lifetime is expected to vary across the PL spectrum of an (In,Ga)N ML system with ML thickness fluctuations, given that the wave function overlap in the different configurations will vary and bearing in mind that also the transition energy depends on the microscopic configuration. Given that the radiative lifetime is tightly linked to the electron and hole wave function overlap, we follow Marquardt *et al.*[46,47] and use the geo-

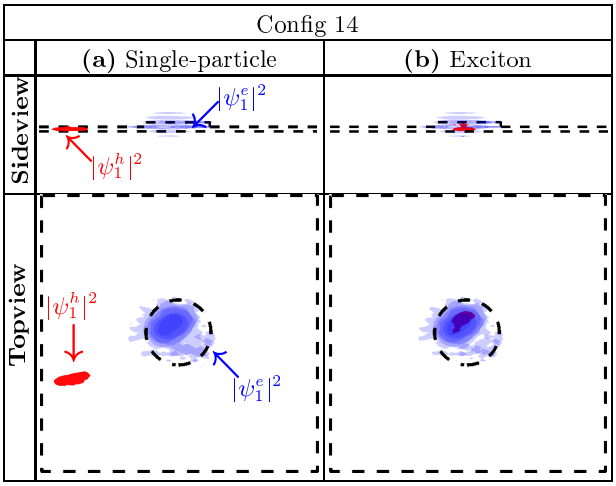


FIG. 10. Isosurface plots of the electron $|\psi^e_{\rm GS}|^2$ (blue) and hole $|\psi^h_{\rm GS}|^2$ (red) ground state charge densities for the microscopic alloy configuration (Config.) 14. In the present case In atoms are allowed to "bleed" into the GaN barrier of the (In,Ga)N monolayer system with 25% In. The isosurfaces are shown at 10% of respective maximum charge density values (Note that the different shades in the isosurface plots of the charge densities originate from overlapping isosurfaces stemming from different planes in c-direction). (a) depicts the single-particle results, while (b) shows the data when including excitonic effects in the calculations. The dashed lines indicate supercell boundary but also the area in which In atoms are allowed to penetrate into the barrier region.

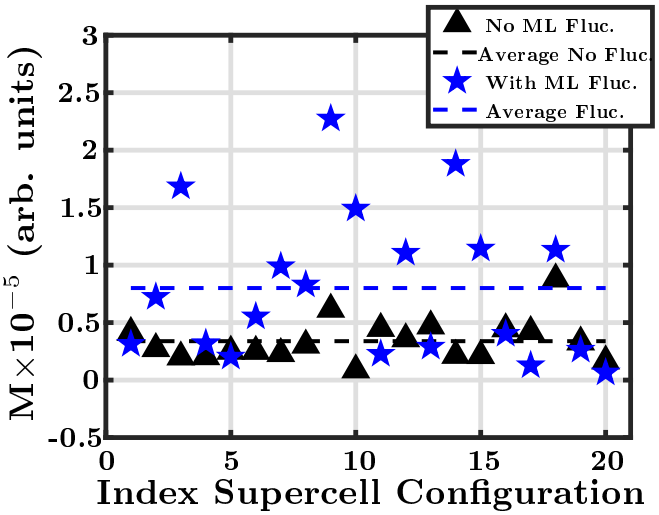


FIG. 11. Electron-hole excitonic charge density overlap as a function of the index of the supercell configurations (alloy configurations). The blue stars give the results in the presence of In atoms penetrating the GaN barrier, while the black triangles represent the data for the atomically "flat" system. The dashed lines give the average overlap values.

metric electron and hole wave function overlap

$$M = \sum_i \rho_e(\mathbf{R}_i)\rho_h(\mathbf{R}_i) \ , \qquad (1)$$

as a measure for the oscillator strength. Here, ρ_e and ρ_h denote the electron and hole excitonic charge densities contribution (including Coulomb effects) at the lattice site $\mathbf{R}_i$ of the supercell. In Fig. 11 the calculated overlap M in the presence of In atoms "bleeding" into the GaN barrier is given by the blue stars and as a function of the index of the supercell configuration; the value averaged over the 20 different configurations is represented by the blue dashed line. To put the impact of the ML width fluctuations on M in perspective, the black triangles give the data in the case of the atomically "flat" system (cf. Fig. 1 (a) and Sec. II B). As Fig. 11 reveals, when introducing ML width fluctuations, the overlap M strongly varies with alloy configuration in contrast to the atomically flat system, where it is almost independent of the alloy configuration. Overall, and as discussed in more detailed investigations on "standard" c-plane (In,Ga)N/GaN QWs, a strong variation in the wave function overlap can manifest itself in non-exponential decay transients in time-resolved PL studies.[31,41] As already mentioned above, such a situation has been experimentally observed in the work by Ma *et al.*[9] and Anikeeva *et al.*[28] on quasi-2D (In,Ga)N ML systems.

Moreover, in the experimental study of Anikeeva *et al.*[28] on ultrathin (In,Ga)N ML systems, an "S"-shape temperature dependence of the PL peak energies has been observed.[28] Such a characteristic is also been widely seen in c-plane (In,Ga)N/GaN systems, and is usually explained by a redistribution of carriers between different localization centers, which exhibit different transition energies. It is interesting to note that in non-polar systems such a behavior is experimentally not observed, and usually attributed to exciton localization effects.[36] Overall, our result of carrier localization and variations in the transition energies due to variations in the local alloy structure are consistent with the experimentally observed "S"-shape temperature dependence of the PL peak energies. Taking then also the observed "indirect exciton" effects into account, arising for instance from small structural inhomogeneities on the order of a ML, deviations from the standard exciton localization picture may be expected. Thus, further supporting that the PL peak energy exhibits a "S"-shape in quasi 2D (In,Ga)N ML systems.

III. CONCLUSIONS

We have theoretically studied the electronic and excitonic properties of ultrathin, monolayer thick wurtzite (In,Ga)N layers embedded in GaN on a microscopic level. Following recent theoretical and experimental studies, the In content in the monolayer was restricted to 25% In. To investigate electronic and optical properties of ultrathin (In,Ga)N systems within an atomistic framework, very large supercells are required to capture the effects of alloy fluctuations. To do so we have applied semi-empirical tight-binding theory in conjunction with

a configuration interaction scheme to capture excitonic effects.

Our investigations show that alloy fluctuations within the (In,Ga)N monolayer lead to strong carrier localization effects. These effects dominate the electronic and optical properties of these ultrathin systems. Our calculations also reveal that the excitonic binding energy is significantly increased in the quasi 2D system when compared to bulk systems of equivalent In content. We find that the calculated average exciton binding energy exceeds the thermal energy at room temperature, so exciton emission at elevated temperatures can be expected in experiment. These theoretical findings are consistent with and shed new light on the literature experimental observations of (i) broad photoluminescence linewidth and (ii) excitonic effects contributing to the radiative recombination process at elevated temperatures. We also find that small structural inhomogeneities, such as local thickness fluctuations of one monolayer, can lead to a spatial separation of electron and holes and in an excitonic picture to "indirect" excitons or *independently* localized electrons and holes. This result is in accordance with the experimentally observed (i) non-exponential decay curves in time resolved photoluminescence spectra and the (ii) "S"-shape temperature dependence of the photoluminescence peak energies. The present work therefore provides on an atomistic level fundamental understanding of the electronic and optical properties of ultrathin, quasi 2D (In,Ga)N monolayers embedded in GaN. At the same time the results are useful to guide the design potential future devices utilizing (In,Ga)N monolayer systems.

IV. METHODS

In this section we provide an overview of the methods applied and the supercells used in the calculations. We start with the discussion of the supercell set up followed by a description of the theoretical framework.

A. Model geometry

To model wurtzite $In_{0.25}Ga_{0.75}N$ ML systems embedded in GaN, we use a supercell with approximately 328,000 atoms and periodic boundary conditions. This corresponds to a supercell size of approximately 20 nm $\times$ 18 nm $\times$ 10 nm. For a cation plane selected near the bottom of the supercell, to account for the fact that built-in field and low effective mass leads to the situation that the electron wave function leaks further into the barrier material along the wurtzite c-axis (z-axis). For the selected cation plane 25% of the Ga cations have been randomly replaced by In atoms. Therefore, we follow the experimental observations that the alloy microstructure of c-plane (In,Ga)N/GaN QWs can be described by a random alloy,[48–50] which is also consistent with the conclusions drawn in Ref.[28]. 20 different microscopic configurations have been constructed; always the same cation plane has been selected to replace Ga by In atoms, so that only the alloy microstructure varies between the different configurations, but not the cation plane. For the ML thick width fluctuations we build again on previous experimental and theoretical data on other c-plane (In,Ga)N systems and treat those as disc-like objects.[22] Typical diameter of these structures are 5-10 nm and heights vary between 1 and 2 ML. In the above studies we have chosen 5 nm for the diameter and 1 ML for the height fluctuations.[22] Thus, our calculations are targeting small structural perturbations, which are motivated always by the lower experimentally reported values when growing GaN on (In,Ga)N QWs, bearing also in mind that for instance the self-limiting growth process discussed in Ref.[28] for ultrathin (In,Ga)N systems suppresses ML fluctuations. Finally, we note that we allow for bleeding of In atoms into the barrier on the "upper interface", based on findings in c-plane (In,Ga)N QWs. Introducing these fluctuations at lower interface in our systems should not change the results significantly, since the hole wave functions are already strongly localized by random alloy fluctuations, as the results in the main text show, and given that the potential drop across the layer is small.

B. Theoretical Framework

Our theoretical framework is based on an atomistic, nearest neighbor sp^3 tight-binding model that has been discussed and benchmarked in detail in Ref.[24,35,51]. While our TB model is parameterized from hybrid-functional density functional theory (DFT) data and has shown very good agreement with DFT data for alloyed systems, different models exist in the literature[52] using different target band structures and thus input data. Therefore, given differences and uncertainties in input parameters (e.g. band offset values)[53] energies of the calculated single-particle states may be affected by this but not the overall features of carrier localization. To obtain the relaxed atomic positions in the supercells discussed above, a valence force field model[51] that includes Coulomb corrections, necessary to describe the elastic properties of highly ionic materials correctly,[54] is applied. Finally, given that (In,Ga)N/GaN heterostructures exhibit very strong electrostatic built-in fields arising from spontaneous and piezoelectric polarization fields, we apply the local polarization theory described in Ref.[51]. Here, the total polarization vector field is separated into contributions arising from macroscopic (clamped ion) and local (internal strain) effects. In the present study we use the piezoelectric coefficients calculated in Ref.[51] for our model. We note that several different parameter sets are available in the literature, which may affect the absolute numbers of the built-in field. However, in general the resulting fields are comparable magnitude, so that overall *trends* should not be significantly affected by choosing

a different parameter set. Once the (local) polarization field is known, we employ a point dipole model to calculate the corresponding built-in potential. Overall, this approach allows us to describe also local fluctuations in the built-in potential on an atomistic level. These (local) corrections are included in the TB Hamiltonian as site-diagonal corrections, which is a widely applied approach in the literature.[55–57]

To address the excitonic properties of the system we apply a configuration interaction (CI) scheme.[58,59] Since we are interested in the excitonic binding energies, which are expected and calculated to be of the order of tens of meV, we have neglected electron hole exchange terms. These terms lead to energy corrections of the order of μeV,[60] and are thus of secondary importance for our studies. For the CI scheme we include the energetically lowest 5 electron and 15 hole states in the expansion, thus taking into account that the energetic separation between different hole states in the (disordered) energy landscape of a given alloy configuration may be (very) small. Even though we take a relatively large number of single-particle states into account, we note that increasing this number may (slightly) affect the excitonic binding energies. Here, the required single particle energies are directly taken from our TB calculations; the Coulomb matrix elements are calculated from the TB wave functions as described in Refs.[45,61], in line with Coulomb matrix element evaluations using TB wave functions carried out by other groups.[62–64] To account for screening of the Coulomb interaction, we take the on-site part to be unscreened while the off-site contributions are screened by the dielectric function;[65,66] we use, similar to Refs.[62,66,67] a constant dielectric function which is taken to be the alloy composition weighted average between the dielectric constants of InN and GaN, bearing in mind that especially the hole wave function is mainly localized in the ML. Using this approach should be a reasonable approximation given that we are interest in (In,Ga)N alloys with relatively low In content (25% In), so that the dielectric mismatch between ML (In,Ga)N material and barrier is not huge. The dielectric constants for InN and GaN have been taken from Ref.[68,69].

CONFLICTS OF INTEREST

There are no conflicts to declare.

ACKNOWLEDGEMENTS

The authors acknowledge the financial support from the Sustainable Energy Authority of Ireland and Science Foundation Ireland under Grant Nos. 17/CDA/4789 and 12/RC/2276 P2.

[1] R. Mas-Balleste, C. Gomez-Navarro, J. Gomez-Herrero and F. Zamora, *Nanoscale*, 2011, **3**, 20.

[2] Y. Ando and L. Fu, *Annu. Rev. Condens. Matter Phys.*, 2015, **6**, 361.

[3] B. Wang, S. Yuan, Y. Li, L. Shi and J. Wang, *Nanoscale*, 2017, **9**, 5577.

[4] W. Chen, X. Gui, L. Yang, H. Zhu and Z. Tang, *Nanoscale Horiz.*, 2019, **4**, 291.

[5] G. Fiori, F. Bonaccorso, G. Iannaccone, T. Palacios, D. Neumaier, A. Seabaugh, S. K. Banerjee and L. Colombo, *Nature Nanotechnology*, 2014, **9**, 768.

[6] A. Castellanos-Gomez, *Nat. Photonics*, 2016, **10**, 202.

[7] T. Akasaka, H. Gotoh, Y. Kobayashi and H. Yamamoto, *Adv. Mater.*, 2012, **24**, 4296.

[8] Z. Y. A. Balushi, K. Wang, R. K. Ghosh, R. A. Vila, S. M. Eichfeld, J. D. Caldwell, X. Qin, Y.-C. Lin, P. A. DeSario, G. Stone, S. Subramanian, D. F. Paul, R. M. Wallace, S. Datta, J. M. Redwing and J. A. Robinson, *Nature Materials*, 2016, **15**, 1166.

[9] D. Ma, X. Rong, X. Zheng, W. Wang, P. Wang, T. Schulz, M. Albrecht, S. Metzner, M. Müller, O. August, F. Bertram, J. Christen, P. Jin, M. Li, J. Zhang, X. Yang, F. Xu, Z. Qin, W. Ge, B. Shen and X. Wang, *Scientific reports*, 2017, **7**, 46420.

[10] N. Sanders, D. Bayerl, G. Shi, K. A. Mengle and E. Kioupakis, *Nano Lett.*, 2017, **17**, 7345.

[11] D. Kecik, A. Onen, M. Konuk, E. Gürbüz, F. Ersan, S. Cahangirov, E. A. E. Durgun and S. Ciraci, *Applied Physics Reviews*, 2018, **5**, 011105.

[12] C. J. Humphreys, *MRS Bulletin*, 2008, **33**, 459.

[13] S. P. DenBaars, D. Feezell, K. Kelchner, S. Pimputkar, C.-C. Pan, C.-C. Yen, S. Tanaka, Y. Zhao, N. Pfaff, R. Farrell, M. Iza, S. Keller, U. Mishra, J. S. Speck and S. Nakamura, *Acta Materialia*, 2013, **61**, 945.

[14] L. Sang, M. Liao, Q. Liang, M. Takeguchi, B. Dierre, B. Shen, T. Sekiguchi, Y. Koide and M. Sumiya, *Adv. Mater.*, 2014, **26**, 1414.

[15] B. AlOtaibi, H. P. T. Nguyen, S. Zhao, M. G. Kibria, S. Fan and Z. Mi, *Nano Lett.*, 2013, **13**, 4356.

[16] A. Yoshikawa, S. B. Che, W. Yamaguchi, H. Saito, X. Q. Wang, Y. Ishitani and E. S. Hwang, *Appl. Phys. Lett.*, 2007, **90**, 073101.

[17] C. Cheze, M. Siekacz, F. Isa, B. Jenichen, F. Feix, J. Buller, T. Schulz, M. Albrecht, C. Skierbiszewski, R. Calarco and H. Riechert, *J. Appl. Phys.*, 2016, **120**, 125307.

[18] P. Wolny, M. Anikeeva, M. Sawicka, T. Schulz, T. Markurt, M. Albrecht, M. Siekacz and C. Skierbiszewski, *J. Appl. Phys.*, 2018, **124**, 065701.

[19] O. Ambacher, J. Majewski, C. Miskys, A. Link, M. Hermann, M. Eickhoff, M. Stutzmann, F. Bernardini, V. Fiorentini, V. Tilak, B. Schaff and L. F. Eastman, *J. Phys.: Condens. Matter*, 2002, **14**, 3399.

[20] C. J. Humphreys, J. T. Griffiths, F. Tang, F. Oehler, S. D. Findlay, C. Zheng, J. Etheridge, T. L.Martin, P. A. J. Bagot, M. P. Moody, D. Sutherland, P. Dawson, S. Schulz, S.Zhang, W. Y. Fu, T. Zhu, M. J. Kappers and R. A. Oliver, *Ultramicroscopy*, 2017, **176**, 93.

[21] L.-W. Wang, *Phys. Rev. B*, 2001, **63**, 245107.

[22] D. Watson-Parris, M. J. Godfrey, P. Dawson, R. A. Oliver, M. J. Galtrey, M. J. Kappers and C. J. Humphreys, *Phys. Rev. B*, 2011, **83**, 115321.

[23] S. Schulz, O. Marquardt, C. Coughlan, M. A. Caro, O. Brandt and E. P. O'Reilly, Proc. SPIE 9357, Physics and Simulation of Optoelectronic Devices XXIII, 2015, p. 93570C.

[24] S. Schulz, M. A. Caro, C. Coughlan and E. P. O'Reilly, *Phys. Rev. B*, 2015, **91**, 035439.

[25] S. F. Chichibu, A. Uedono, T. Onuma, B. A. Haskell, A. Chakraborty, T. Koyama, P. T. Fini, S. Keller, S. P. DenBaars, J. S. Speck, U. K. Mishra, S. Nakamura, S. Yamaguchi, S. Kamiyama, H. Amano, I. Akasaki, J. Han and T. Sota, *Nature Mater.*, 2006, **5**, 810.

[26] E. Kioupakis, Q. Yan and C. G. Van de Walle, *New J. Phys.*, 2013, **15**, 125006.

[27] L. Lymperakis, T. Schulz, C. Freysoldt, M. Anikeeva, Z. Chen, X. Zheng, B. Shen, C. Cheze, M. Siekacz, X. Q. Wang, M. Albrecht and J. Neugebauer, *Phys. Rev. Materials*, 2018, **2**, 011601(R).

[28] M. Anikeeva, M. Albrecht, F. Mahler, J. W. Tomm, L. Lymperakis, C. Chee, R. Calarco, J. Neugebauer and T. Schulz, *Scientific reports*, 2019, **9**, 9047.

[29] F. Fedichkin, T. Guillet, P. Valvin, B. Jouault, C. Brimont, T. Bretagnon, L. Lahourcade, N. Grandjean, P. Lefebvre and M. Vladimirova, *Phys. Rev. Appl.*, 2016, **6**, 014011.

[30] E. V. Calman, M. M. Fogler, L. V. Butov, S. Hu, A. Mishchenko and A. K. Geim, *Nature Comm.*, 2018, **9**, 1895.

[31] A. Morel, P. Lefebvre, S. Kalliakos, T. Taliercio, T. Bretagnon and B. Gil, *Phys. Rev. B*, 2003, **68**, 045331.

[32] I. Vurgaftman and J. R. Meyer, *J. Appl. Phys.*, 2003, **94**, 3675.

[33] M. Dvorak, S. H. Wei and Z. Wu, *Phys. Rev. Lett.*, 2013, **110**, 169904.

[34] M. S. Prete, O. Pulci and F. Bechstedt, *Phys. Rev. B*, 2018, **98**, 235431.

[35] D. S. P. Tanner, P. Dawson, M. J. Kappers, R. A. Oliver and S. Schulz, *Phys. Rev. Applied*, 2020, **13**, 044068.

[36] S. Schulz, D. P. Tanner, E. P. O'Reilly, M. A. Caro, T. L. Martin, P. A. J. Bagot, M. P. Moody, F. Tang, J. T. Griffiths, F. Oehler, M. J. Kappers, R. A. Oliver, C. J. Humphreys, D. Sutherland, M. J. Davies and P. Dawson, *Phys. Rev. B*, 2015, **92**, 235419.

[37] P. R. C. Kent and A. Zunger, *Phys. Rev. B*, 2001, **64**, 115208.

[38] P. Rinke, M. Winkelnkemper, A. Qteish, D. Bimberg, J. Neugebauer and M. Scheffler, *Phys. Rev. B*, 2008, **77**, 075202.

[39] S. Schulz, T. J. Badcock, M. A. Moram, P. Dawson, M. J. Kappers, C. J. Humphreys and E. P. O'Reilly, *Phys. Rev. B*, 2010, **82**, 125318.

[40] S. Marcinkevičius, K. M. Kelchner, L. Y. Kuritzky, S. Nakamura, S. P. DenBaars and J. S. Speck, *Appl. Phys. Lett.*, 2013, **103**, 111107.

[41] P. Dawson, S. Schulz, R. A. Oliver, M. J. Kappers and C. J. Humphreys, *J. Appl. Phys.*, 2016, **119**, 181505.

[42] F. Massabuau, N. Piot, M. Frentrup, X. Wang, Q. Avenas, M. Kappers, C. Humphreys and R. Oliver, *Phys. Status Solidi B*, 2017, **254**, 1600664.

[43] M. J. Galtrey, R. A. Oliver, M. J. Kappers, C. J. Humphreys, P. Clifton, D. Larson, D. Saxey and A. Cerezo, *J. Appl. Phys.*, 2008, **104**, 013524.

[44] M. A. Moram and M. E. Vickers, *Rep. Prog. Phys.*, 2009, **72**, 036502.

[45] S. Schulz, S. Schumacher and G. Czycholl, *Phys. Rev. B*, 2006, **73**, 245327.

[46] O. Marquardt, C. Hauswald, M. Wölz, L. Geelhaar and O. Brandt, *Nano Lett.*, 2013, **13**, 3298.

[47] O. Marquardt, L. Geelhaar and O. Brandt, *Nano Lett.*, 2015, **15**, 4289.

[48] J. P. O'Neill, I. M. Ross, A. G. Cullis, T. Wang and P. J. Parbrook, *Appl. Phys. Lett.*, 2003, **83**, 1965.

[49] T. M. Smeeton, M. J. Kappers, J. S. Barnard, M. E. Vickers and C. J. Humphreys, *Appl. Phys. Lett.*, 2003, **83**, 5419.

[50] D. M. Graham, A. Soltani-Vala, P. Dawson, M. J. Godfrey, T. M. Smeeton, J. S. Barnard, M. J. Kappers, C. J. Humphreys and E. J. Thrush, *J. Appl. Phys.*, 2005, **97**, 103508.

[51] M. A. Caro, S. Schulz and E. P. O'Reilly, *Phys. Rev. B*, 2013, **88**, 214103.

[52] M. Auf der Maur, A. Pecchia, G. Penazzi, W. Rodrigues and A. Di Carlo, *Phys. Rev. Lett.*, 2016, **116**, 027401.

[53] P. G. Moses, M. Miao, Q. Yan and C. G. Van de Walle, *J. Chem. Phys.*, 2011, **134**, 084703.

[54] D. S. P. Tanner, M. A. Caro, S. Schulz and E. P. O'Reilly, *Phys. Rev. B*, 2019, **100**, 094112.

[55] T. Saito and Y. Arakawa, *Physica E (Amsterdam)*, 2002, **15**, 169.

[56] M. Zielinski, W. Jaskolski, J. Aizpurua and G. W. Bryant, *Acta Physica Polonica A*, 2005, **108**, 929.

[57] K. Schuh, S. Barthel, O. Marquardt, T. Hickel, J. Neugebauer, G. Czycholl and F. Jahnke, *Appl. Phys. Lett.*, 2012, **100**, 092103.

[58] A. Franceschetti, H. Fu, L. W. Wang and A. Zunger, *Phys. Rev. B*, 1999, **60**, 1819.

[59] N. Baer, S. Schulz, S. Schumacher, P. Gartner, G. Czycholl and F. Jahnke, *Appl. Phys. Lett.*, 2005, **87**, 231114.

[60] S. K. Patra and S. Schulz, *Nano Lett.*, 2020, **20**, 234.

[61] D. S. P. Tanner, J. M. McMahon and S. Schulz, *Phys. Rev. Applied*, 2018, **10**, 034027.

[62] W. Sheng, S. J. Cheng and P. Hawrylak, *Phys. Rev. B*, 2005, **71**, 035316.

[63] M. Zielinski, M. Korkusinski and P. Hawrylak, *Phys. Rev. B*, 2010, **81**, 085301.

[64] D. Mourad, A. Guille, T. Aubert, E. Brainis and Z. Hens, *Chemistry of Materials*, 2014, **26**, 6852.

[65] M. Korkusinski, O. Voznyy and P. Hawrylak, *Phys. Rev. B*, 2010, **82**, 245304.

[66] M. Swiderski and M. Zielinski, *Phys. Rev. B*, 2017, **95**, 125407.

[67] E. Goldmann, S. Barthel, M. Florian, K. Schuh and F. Jahnke, *Appl. Phys. Lett.*, 2013, **103**, 242102.

[68] S. Nakamura and S. Chichibu, *Introduction to Nitride Semiconductor Blue Lasers and Light Emitting Diodes*, Taylor & Francis, London, 2000.

[69] V. Y. Davydov, A. A. Klochikhin, M. B. Smirnov, V. V.Emtsev, V. D. Petrikov, I. A.Abroyan, A. I. Titov, I. N. Goncharuk, A. N. Smirnov, V. V. Mamutin, S. V. Ivanov and T. Inushima, *Phys. Status Solidi B*, 1999, **216**, 779.